LETTERS

A climatologically significant aerosol longwave indirect effect in the Arctic

Dan Lubin[1]* & Andrew M. Vogelmann[2]*

The warming of Arctic climate and decreases in sea ice thickness and extent[1,2] observed over recent decades are believed to result from increased direct greenhouse gas forcing, changes in atmospheric dynamics having anthropogenic origin[3–5], and important positive reinforcements including ice–albedo and cloud–radiation feedbacks[6]. The importance of cloud–radiation interactions is being investigated through advanced instrumentation deployed in the high Arctic since 1997 (refs 7, 8). These studies have established that clouds, via the dominance of longwave radiation, exert a net warming on the Arctic climate system throughout most of the year, except briefly during the summer[9]. The Arctic region also experiences significant periodic influxes of anthropogenic aerosols, which originate from the industrial regions in lower latitudes[10]. Here we use multisensor radiometric data[7,8] to show that enhanced aerosol concentrations alter the microphysical properties of Arctic clouds, in a process known as the 'first indirect' effect[11,12]. Under frequently occurring cloud types we find that this leads to an increase of an average 3.4 watts per square metre in the surface longwave fluxes. This is comparable to a warming effect from established greenhouse gases and implies that the observed longwave enhancement is climatologically significant.

We use five data sets from the North Slope of Alaska (NSA) site, established by US Department of Energy Atmospheric Radiation Measurement (ARM) program[7], to determine the impact of aerosol on Arctic cloud microphysics and the surface longwave budget. The Atmospheric Emitted Radiance Interferometer (AERI)[13] is a Fourier transform infrared spectroradiometer that measures downwelling zenith sky radiance in the wavelength range 3.3–25 μm (400–3,020 cm^{-1}), with a spectral resolution of 1 cm^{-1} and a radiometric calibration accuracy of 1%. The Active Remotely Sensed Cloud Locations (ARSCL)[14] data set combines ceilometer, lidar and millimetre wave cloud radar measurements to determine the vertical location of cloud layers. Downwelling hemispheric longwave flux is measured by pyrgeometers with an accuracy of ±5% (ref. 15). A NOAA Climate Modelling and Diagnostics Laboratory (CMDL) facility[16] is adjacent to the ARM NSA site in Barrow, Alaska, and provides measurements of aerosol condensation nuclei (CN) concentrations at the surface. The CN measurements indicate times when substantial aerosol abundances are present and may have the potential to serve as cloud condensation nuclei in low stratus cloud in the Arctic[17]. Rawinsondes are launched approximately five days a week from the NSA site and, in conjunction with the ARSCL data, these soundings provide estimates of cloud base temperature. We analysed six years of the ARM NSA and CMDL data (1998–2003).

AERI spectral measurements in the middle infrared are sensitive to cloud droplet size[18–20], and therefore to the aerosol indirect effect. Radiative transfer calculations[19] (Fig. 1a) illustrate how the zenith radiance under a cloud with fixed liquid water path, LWP, varies with the effective radius of the droplet size distribution[18,20], r_e. As r_e decreases, the effective brightness temperature (T_b) increases in the wavenumber (υ) interval 800–1,000 cm^{-1}, and the slope of the spectral brightness temperature, $dT_b/d\upsilon$, decreases (becomes more negative). This results from changes in cloud emissivity (Fig. 1b); as r_e decreases, emissivity generally increases and, also, its spectral dependence increases within the 800–1,000 cm^{-1} spectral interval. Figure 1c illustrates the effect of these spectral cloud properties on the downwelling longwave flux at the Arctic Earth surface. For a fixed LWP, a decrease in r_e yields a smaller $dT_b/d\upsilon$ and a larger downwelling longwave flux. For large LWP, the cloud radiates as a blackbody and the spectral and longwave sensitivities vanish[18]. Our approach here is to: (1) detect the aerosol indirect effect by observing whether AERI spectral brightness temperatures indicate a significant shift towards smaller (more negative) $dT_b/d\upsilon$ in the presence of high CN concentrations; (2) verify a concomitant increase in cloud emissivity, manifested as a larger downwelling flux measured in the pyrgeometer data; (3) quantify the importance of the magnitude of this enhancement to the surface longwave radiation budget; and (4) determine the portion of this longwave enhancement that is due to systematic changes in r_e.

Our analysis indicates a clear tendency for AERI $dT_b/d\upsilon$ to decrease in the presence of larger CN, consistent with smaller r_e and the aerosol indirect effect. Our approach is illustrated in Fig. 2, which shows two AERI spectra observed under clouds with the same geometrical properties, but which have greatly differing CN concentrations. Consistent with our theoretical discussion, the measured $dT_b/d\upsilon$ between 800 and 1,000 cm^{-1} is clearly more negative for the high CN case. From this spectral information, it is also possible to directly retrieve r_e and LWP from AERI data[18,21], because the spectral radiance in the interval 800–1,000 cm^{-1} is sensitive to r_e, while the spectral radiance in the interval 1,100–1,250 cm^{-1} is sensitive to LWP/r_e. From the examples of Fig. 2, we retrieve LWP = 15.4 g m^{-2} and r_e = 11 μm for the low CN case, and LWP = 13.5 g m^{-2} and r_e = 7 μm for the high CN case.

Our detection technique involving $dT_b/d\upsilon$ was applied to the full six-year data set by collocating individual AERI emission spectra with hourly-averaged CN measurements. The ARSCL data set was used to select all periods when single-layer clouds with base heights and geometric thickness under 1,000 m occurred over surface temperatures between 265 and 280 K. These selection rules favour liquid water clouds. Liquid water was recently discovered to largely govern Arctic cloud radiative properties during spring and summer[22], with liquid water being found in clouds at temperatures as low as −34 °C (ref. 23). From the AERI measurements, we determined the brightness temperature slope in the interval 800–1,000 cm^{-1}, $dT_b/d\upsilon$. The CN measurements were screened by wind direction to remove local effects from Barrow. The slopes were sorted by the coincident CN concentration, where 'low' CN are <50 cm^{-3} and 'high' are

[1]Scripps Institution of Oceanography, University of California San Diego, La Jolla, California 92093-0221, USA. [2]Brookhaven National Laboratory, Upton, New York 11973, USA.
*These authors contributed equally to this work.

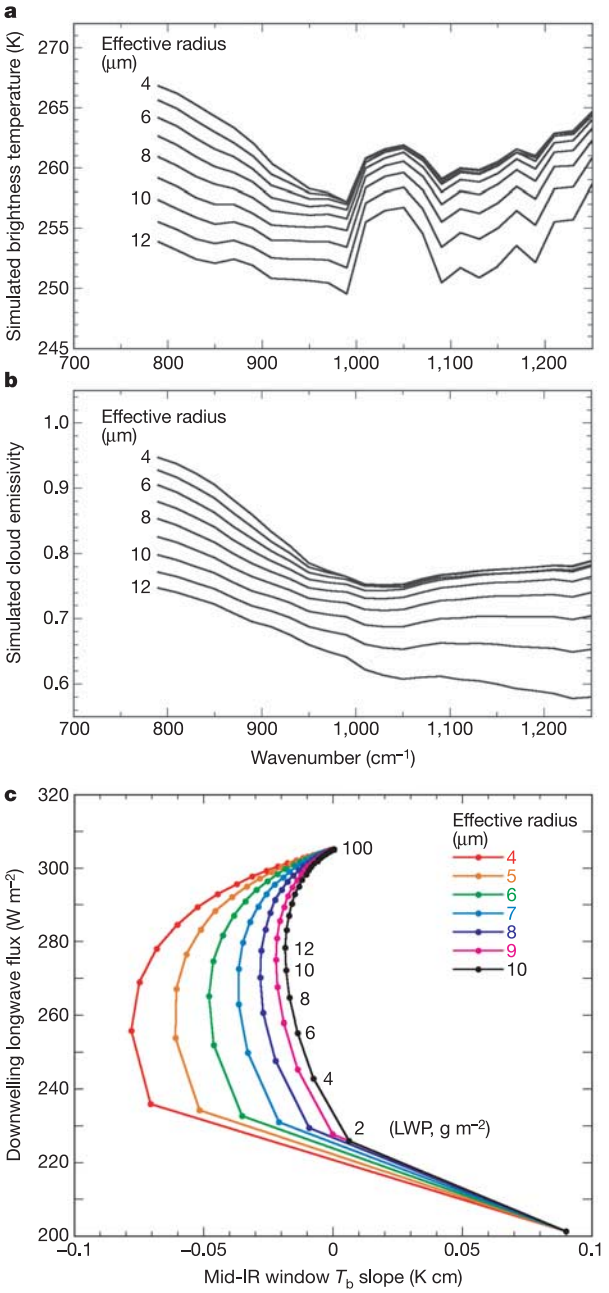

Figure 1 | Demonstration of how surface longwave flux under cloud depends on cloud liquid water path and effective radius. **a**, Radiative transfer simulations[19] of the spectral dependence of effective scene temperature, or 'brightness temperature' (T_b), corresponding to downwelling zenith radiance under a liquid water cloud. The cloud liquid water path (LWP) is held constant at 12 g m^{-2} and the effective radius (r_e) is varied from 4 to 12 μm, a range commonly observed in terrestrial water clouds. **b**, The spectral cloud emissivity from the calculation in **a**. **c**, Radiative transfer simulation of the downwelling broadband longwave flux as a function of the brightness temperature slope dT_b/dυ in the interval 800–1,000 cm^{-1}, plotted as curves of fixed r_e with LWP increasing as indicated.

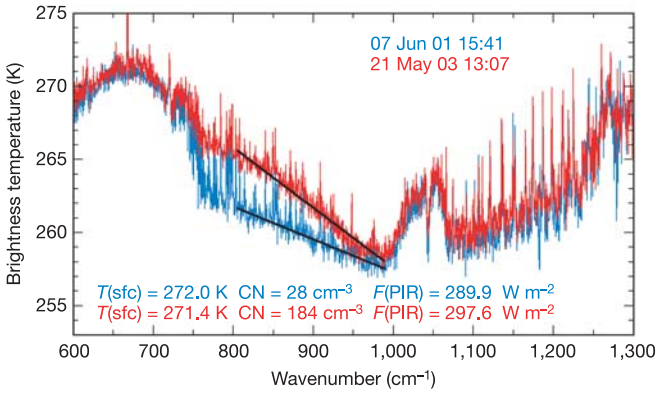

Figure 2 | Examples of AERI measurements. Downwelling emission spectra measured by the NSA AERI beneath two clouds with very different condensation nuclei (CN) concentrations. Near-surface (2 m) air temperature T(sfc) and pyrgeometer-measured downwelling longwave flux F(PIR) are also indicated.

>175 cm^{-3}. These thresholds were chosen on the basis of the lowest and highest 25th percentiles for all CN data, respectively, and they are also consistent with other Arctic studies[17,24]. From the six-year data set subsampled as described, we found 2,379 collocated low CN cases and 5,164 high CN cases. Analysing these cases revealed a systematic tendency for dT_b/dυ to be more negative under high CN than under low CN, consistent with the aerosol indirect effect causing smaller r_e.

The effects of elevated CN concentrations on the downwelling longwave radiation are investigated by collocating the instantaneous pyrgeometer fluxes with the AERI-measured dT_b/dυ (Fig. 3a); the relationship between these measured quantities is highly consistent with theoretical expectations (Fig. 1c). For dT_b/dυ < 0, the high CN points clearly exhibit a greater spread towards more negative slopes, and their maximum downwelling pyrgeometer fluxes are greater than for the low CN points. Larger flux for higher CN is consistent with the theorized increase in cloud emissivity for smaller r_e.

This result is better quantified by binning the pyrgeometer fluxes in dT_b/dυ bins of width 0.01 K cm^{-1} (0.005 K cm^{-1} near dT_b/dυ = 0) and computing the mean and standard deviations of the fluxes per bin. Two-sample t-tests are performed for each dT_b/dυ bin to determine whether the high and low CN cases comprise statistically significant different distributions. Figure 3b shows that, for the same dT_b/dυ bin, the pyrgeometer fluxes for high CN are consistently greater than for low CN. The statistical significance is above the 99% confidence level for all but one of the dT_b/dυ bins. For the dT_b/dυ = 0 bin (rightmost pair of data points), no significant difference exists between the high and low CN cases, consistent with most of those clouds having optical depth greater than ~10 and radiating as blackbodies[18]. Considering all six years of the low, single-layer stratiform clouds at the NSA, we find that the mean pyrgeometer downwelling flux measured for the high CN cases is 8.2 W m^{-2} greater than for the low CN cases.

We now show that our observed flux difference between the high and low CN cases (Fig. 3b) is not an artefact of additional seasonal considerations or temperature effects. We examine a subset of the springtime data (May and June), for which cloud optical depths have been found to be similar in a recent climatological study[25], and for surface temperatures confined to the range 267–274 K (in addition to the above selection rules). This subset contains 1,068 collocated low CN and 1,289 high CN cases. Available rawinsonde data covering this data subset indicate average near-surface air temperatures of 272.4 ± 1.2 K and 272.3 ± 1.9 K for the low and high CN cases, respectively, and cloud base temperatures of 270.4 ± 3.3 K and 269.6 ± 9.1 K for the low and high CN cases, respectively. We first sorted this data subset on dT_b/dυ (Fig. 3c), and determined that the mean pyrgeometer downwelling flux measured for these high CN cases is 12.3 W m^{-2} greater than for the corresponding low CN cases, when we exclude the blackbody cases in the dT_b/dυ = 0 bin. We then retrieved r_e and LWP from all AERI spectra having dT_b/dυ < 0 in this data subset[18,21]. Figure 3d indicates a most probable r_e of 10 μm under low CN and 6 μm under high CN.

To determine the amount of the total flux difference between these low and high CN cases that is due to this systematic difference in r_e,

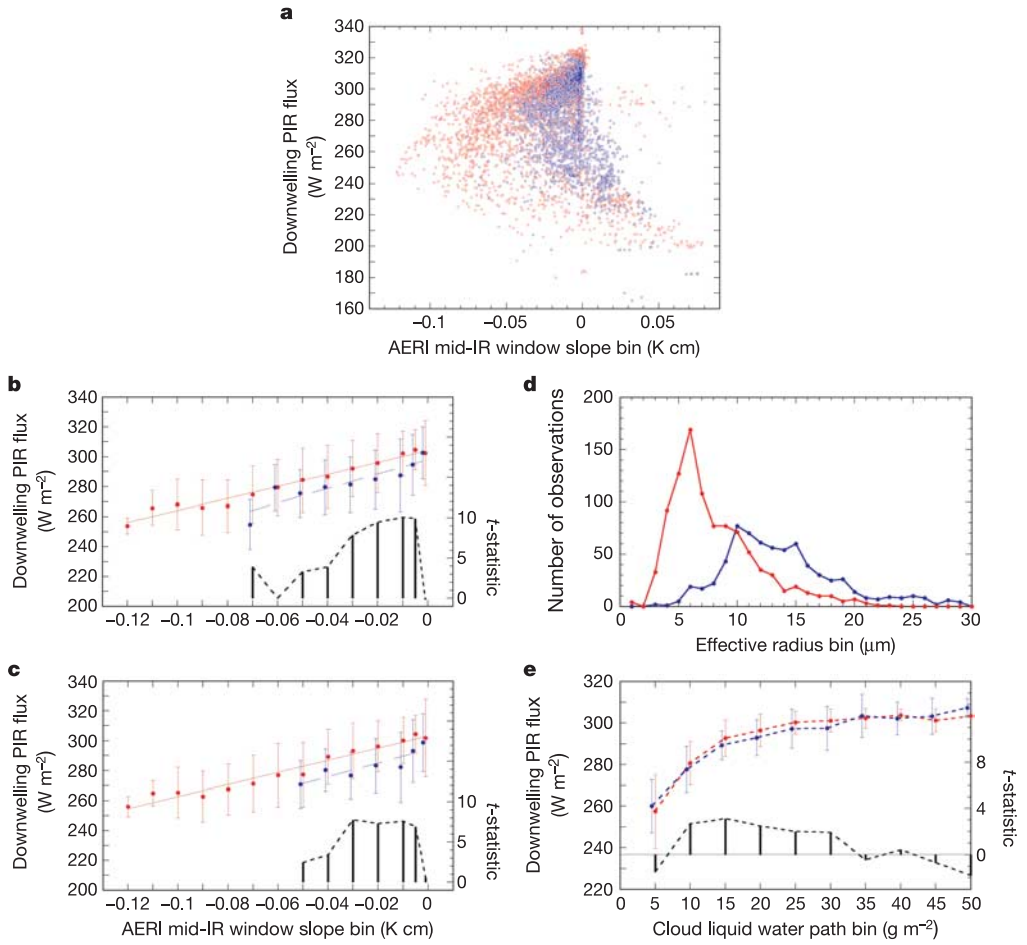

Figure 3 | Demonstration of the aerosol longwave indirect effect from ARM NSA data. a–c, The downwelling longwave flux measured by NSA pyrgeometers (Precision Infrared Radiometer, PIR) under single-layer clouds as a function of the AERI-measured $dT_b/d\upsilon$: **a**, instantaneous measurements for all low and high CN cases; **b**, downwelling flux averages and standard deviations (1σ) in $dT_b/d\upsilon$ bins of width 0.01 K cm (width 0.005 near $dT_b/d\upsilon = 0$) for all low and high CN cases; **c**, as in **b** but for a data subset comprising May and June only, and surface temperature range 267–274 K. **d**, Histograms of AERI-retrieved r_e under low and high CN from the May–June subset. **e**, Pyrgeometer bin averages as in **c** for the May–June subset, but sorted on LWP bins of width 5 g m^{-2}. Statistics from 2-sample *t*-tests indicate the bins where significant differences exist between the contrasted sample means for the high and low CN concentrations.

we sorted the May–June data subset in LWP bins of width 5 g m^{-2} (Fig. 3e). Statistically significant flux differences emerge throughout most of the LWP range for which $dT_b/d\upsilon < 0$. With this constant-LWP sorting, the mean pyrgeometer flux in a given LWP bin under high CN is on average 3.4 W m^{-2} larger than under low CN. The remaining flux difference between the cases might be an effect of greater LWP under high CN. An increase in cloud LWP in the presence of increased aerosol concentrations would be consistent with recent theoretical work on Arctic cloud microphysics[26,27]; however, the current analysis does not allow a rigorous evaluation of atmospheric states that would enable us to firmly demonstrate this additional effect.

In conclusion, we provide observational evidence that the first aerosol indirect effect operates in low, optically thin, single-layered Arctic clouds with a concomitant increase in the downwelling longwave flux. The cloud amount during the Arctic spring generally exceeds 80% (ref. 9), which implies that the observed longwave enhancement has climatological significance.

Received 21 June; accepted 14 November 2005.

1. Moritz, R. E., Bitz, C. M. & Steig, E. J. Dynamics of recent climate change in the Arctic. *Science* **297,** 1497–1502 (2002).
2. Cavalieri, D. J., Gloersen, P., Parkinson, C. L., Comiso, J. C. & Zwally, H. J. Observed hemispheric asymmetry in global sea ice changes. *Science* **278,** 1104–1106 (1997).
3. Thompson, D. W. J. & Wallace, J. M. Annular modes in the extratropical circulation. Part I: month-to-month variability. *J. Clim.* **13,** 1000–1016 (2001).
4. Rigor, I. G., Wallace, J. W. & Colony, R. L. Response of sea ice to the Arctic Oscillation. *J. Clim.* **15,** 2648–2663 (2002).
5. Johanessen, O. M. *et al.* Arctic climate change: observed and modelled temperature and sea ice variability. *Tellus A* **56,** 328–341 (2004).
6. Curry, J. A. & Webster, P. J. *Thermodynamics of Atmospheres and Oceans* (Academic, San Diego, 1999).
7. Stamnes, K., Ellingson, R. G., Curry, J. A., Walsh, J. E. & Zak, B. D. Review of science issues, deployment strategy, and status for the ARM North Slope of Alaska–Adjacent Arctic Ocean climate research site. *J. Clim.* **12,** 46–63 (1999).
8. Uttal, T. *et al.* Surface heat budget of the Arctic Ocean. *Bull. Am. Meteorol. Soc.* **83,** 255–275 (2002).
9. Intrieri, J. M., Shupe, M. D., Uttal, T. & McCarty, B. J. An annual cycle of Arctic cloud characteristics observed by radar and lidar at SHEBA. *J. Geophys. Res.* **107,** doi:10.1029/2000JC000423 (2002).
10. Barrie, L. A. Arctic air pollution: an overview of current knowledge. *Atmos. Environ.* **20,** 643–663 (1986).
11. Twomey, S. The influence of pollution on the shortwave albedo of clouds. *J. Atmos. Sci.* **34,** 1149–1152 (1977).
12. Garrett, T., Radke, L. F. & Hobbs, P. V. Aerosol effects on cloud emissivity and surface longwave heating in the Arctic. *J. Atmos. Sci.* **59,** 769–778 (2002).
13. Knuteson, R. O. *et al.* Atmospheric Emitted Radiance Interferometer. Part II: instrument performance. *J. Ocean. Atmos. Technol.* **21,** 1777–1789 (2004).
14. Clothiaux, E. E. *et al.* Objective determination of cloud heights and radar reflectivities using a combination of active remote sensors at the ARM CART sites. *J. Appl. Meteorol.* **39,** 645–665 (2000).
15. Payne, R. E. & Anderson, S. P. A new look at calibration and use of Eppley Precision Infrared Radiometer, Part II: calibration and use of the Woods Hole

Oceanographic Institution improved meteorology precision infrared radiometer. *J. Ocean. Atmos. Technol* **16,** 739–751 (1999).
16. Delene, D. J. & Ogren, J. A. Variability of aerosol optical properties at four North American surface monitoring sites. *J. Atmos. Sci.* **59,** 1135–1150 (2002).
17. Garrett, T. J., Zhao, C., Dong, X., Mace, G. G. & Hobbs, P. V. Effects of varying aerosol regimes on low-level Arctic stratus. *Geophys. Res. Lett.* **31,** doi:10.1029/2004GL019928 (2004).
18. Turner, D. D. Arctic mixed-phase cloud properties from AERI lidar observations: Algorithm and results from SEHBA. *J. Appl. Meteorol.* **44,** 427–444 (2005).
19. Lubin, D. Thermodynamic phase of maritime Antarctic clouds from FTIR and supplementary radiometric data. *J. Geophys. Res.* **109,** doi:10.1029/2003JD003979 (2004).
20. Mahesh, A., Walden, V. P. & Warren, S. G. Ground-based infrared remote sensing of cloud properties over the Antarctic Plateau. Part II: cloud optical depths and particle sizes. *J. Appl. Meteorol.* **40,** 1279–1294 (2001).
21. Guo, G., Ji, Q., Yang, P. & Tsay, S.-C. Remote sensing of cirrus optical and microphysical properties from ground-based infrared radiometric measurements—Part II: Retrievals from CRYSTAL-FACE measurements. *IEEE Geosci. Rem. Sens. Lett.* **2,** 132–135 (2005).
22. Shupe, M. D. & Intrieri, J. M. Cloud radiative forcing of the Arctic surface: the influence of cloud properties, surface albedo, and solar zenith angle. *J. Clim.* **17,** 616–628 (2004).
23. Intrieri, J. M. *et al.* An annual cycle of surface cloud forcing at SHEBA. *J. Geophys. Res.* **107,** doi:10.1029/2000JC000439 (2002).
24. Penner, J. E., Dong, X. & Chen, Y. Observational evidence of a change in radiative forcing due to the aerosol indirect effect. *Nature* **427,** 231–234 (2004).
25. Leontyeva, E. & Stamnes, K. Estimations of cloud optical thickness from ground-based measurements of incoming solar radiation in the Arctic. *J. Clim.* **7,** 566–578 (1994).
26. Jiang, H. J., Feingold, G., Cotton, W. R. & Duynkerke, P. G. Large-eddy simulations of entrainment of cloud condensation nuclei into the Arctic boundary layer: May 18, 1998, FIRE/SHEBA case study. *J. Geophys. Res.* **106,** 15113–15122 (2001).
27. Morrison, H., Curry, J. A., Shupe, M. D. & Zuidema, P. A new double-moment microphysics parameterization for application in cloud and climate models. Part II: Single-column modeling of arctic clouds. *J. Atmos. Sci.* **62,** 1678–1693 (2005).

Acknowledgements This work was supported by the DOE ARM programme. We thank J. Ogren for access to the NOAA CMDL aerosol data.

Author Information Reprints and permissions information is available at npg.nature.com/reprintsandpermissions. The authors declare no competing financial interests. Correspondence and requests for materials should be addressed to D.L. (dlubin@ucsd.edu).